Supporting Information for

Organophosphonate-degrading PhnZ reveals an emerging family of HD-domain mixed-valent diiron oxygenases

Bigna Wörsdörfer,[1,*] Mahesh Lingaraju,[2] Neela Yennawar,[3] Amie K. Boal,[1,2] Carsten Krebs,[1,2] J. Martin Bollinger, Jr.,[1,2,*] Maria-Eirini Pandelia[1,*]

[1]Department of Chemistry, [2]Department of Biochemistry and Molecular Biology, and [3]Huck Institutes of the Life Sciences, The Pennsylvania State University, University Park, PA 16802, USA

*Corresponding authors:

mpandelia@gmail.com; jmb21@psu.edu; bigna.woe@gmail.com

Materials

Buffers, salts and other chemicals were purchased from commercial suppliers unless otherwise stated. Metallic ^{57}Fe was purchased from Isoflex (USA).

Protein production and purification

The genes for PhnZ (GeneBank ID: ACU83550) and PhnY (GeneBank ID: ACU83549) were codon-optimized for expression in *E. coli*, synthesized, and inserted into the plasmid pRSET_A_A185 at its *XhoI* and *EcoRI* restriction sites by GeneArt. The resulting plasmids pRSET*_phnZ* and pRSET*_phnY* encode the PhnZ and PhnY proteins with N-terminal His_6-tags. For PhnY, the codon-optimized gene was PCR amplified from the purchased pRSET*_phnY* plasmid and subcloned into a pET28a vector using *NdeI* and *XhoI* restriction enzymes, resulting in the plasmid pET28a*_phnY* encoding the *phnY* gene with an N-terminal His_6-tag.

PhnZ was overexpressed in *E. coli* BL21 cells that had been transformed with the plasmid pRSET*_phnZ*. Cultures were grown at 30 °C in enriched LB medium supplemented with ampicillin (0.15 mg/mL) to an OD_{600} of 0.7, at which point PhnZ production was induced by addition of isopropyl-β-D-1-thiogalactopyranoside (IPTG) to 0.5 mM. 4 hours after induction, the cells were harvested by centrifugation at 6,000 *g* for 15 min at 4 °C. To obtain ^{57}Fe-labeled PhnZ for Mössbauer spectroscopy, *E. coli* BL21 cells containing the plasmid pRSET*_phnZ* were grown in M9 minimal medium (with 0.4% (w/v) glucose) supplemented with ampicillin (0.15 mg/mL) and 100 µM $^{57}Fe^{II}$ at 37 °C to an OD_{600} of 0.7, at which point PhnZ production was induced by addition of IPTG to 0.5 mM and the temperature was reduced to 18 °C. 20 to 24 hours after induction, the cells were harvested by centrifugation. The cell mass was resuspended in 4 mL/g lysis buffer (50 mM MOPS pH 7.5, 300 mM NaCl, 10 mM imidazole) supplemented with 1 mM phenylmethylsulfonyl fluoride (PMSF), and the cells were lysed by two passages through a French Pressure cell. The cell lysate was cleared by centrifugation at 22,000 *g* for 30 min at 4 °C and loaded onto a gravity flow Ni^{2+}-NTA agarose (Macherey-Nagel) column that had been equilibrated with lysis buffer. After the column was washed with 2 column volumes (CV) lysis buffer, 2 CV lysis buffer containing 20 mM imidazole, and 2 CV lysis buffer containing 40 mM imidazole, PhnZ was eluted with buffer containing 50 mM MOPS pH 7.5, 100 mM NaCl, and 250 mM imidazole.

For overexpression of PhnY, *E. coli* BL21 cells that had been transformed with the plasmid pET28a*_phnY* were grown at 30 °C in enriched LB medium supplemented with kanamycin (0.05 mg/mL) to an OD_{600} of 0.7, at which point PhnY production was induced by addition of IPTG to 0.1 mM and the temperature was reduced to 15 °C. 25 hours after induction, the cells were

harvested by centrifugation at 6,000 *g* for 15 min at 4 °C. Cleared cell lysate was prepared as described for PhnZ and loaded onto a gravity flow Ni^{2+}-NTA agarose (Macherey-Nagel) column that had been equilibrated with lysis buffer. After the column was washed with 2 CV lysis buffer and 2 CV lysis buffer containing 40 mM imidazole, PhnY was eluted with buffer containing 50 mM MOPS pH 7.5, 100 mM NaCl, and 250 mM imidazole.

The eluted proteins were concentrated in Centriprep YM-10 centrifugal concentrators (Millipore) and exchanged into MOPS buffer (50 mM MOPS pH 7.5, 10% (v/v) glycerol) using a PD-10 column (GE Healthcare). Protein purity was assessed by SDS-PAGE, and protein concentrations were determined using ε_{280nm} = 31.4 mM^{-1} cm^{-1} for PhnZ and ε_{280nm} = 48.36 mM^{-1} cm^{-1} for PhnY as determined on the basis of the amino acid sequence by the ProtParam tool of ExPASy (http://web.expasy.org/protparam/) (1). The Fe content was determined by ferrozine assay (2). Iron and other trace metals in the samples were quantified by inductively-coupled plasma atomic emission spectroscopy (ICP-AES) by Henry Gong at the Penn State Materials Characterization Laboratory (3). PhnZ typically contained 1.2 ± 0.2 Fe per monomer and no significant quantities of other divalent metals.

Enzymatic synthesis of 2-amino-1-hydroxyethylphosphonate by PhnY

The 200 mL reaction contained 5 µM PhnY, 10 µM $Fe(NH_4)_2(SO_4)_2$, 3 mM α-ketoglutarate (α-KG), 100 µM sodium L-ascorbate, and 2 mM 2-aminoethylphosphonate (2-AEP) in 25 mM ammonium acetate buffer pH 7.5. Initially, PhnY was added to an O_2-free mixture of the $Fe(NH_4)_2(SO_4)_2$, L-ascorbate, α-KG, and 2-AEP in 26 mL ammonium acetate buffer after adjusting the pH to 7.5 with concentrated ammonium hydroxide (NH_4OH). The reaction was transferred outside the anoxic chamber, initiated by the addition of 174 mL air-saturated ammonium acetate buffer, and then continuously flushed with hydrated air under gentle stirring at room temperature. Conversion of 2-AEP to 2-amino-1-hydroxyethylphosphonate (OH-AEP) was monitored by ^{31}P-NMR: 480 µL aliquots were taken and quenched by heating to 85 °C for 15 min, and NMR samples were prepared as described in the ^{31}P-NMR spectroscopy section below. After complete conversion of 2-AEP to OH-AEP, the reaction was quenched by incubation at 80 °C for 20 min, and the precipitate was removed by centrifugation at 7,500 × *g* for 15 min at 4 °C followed by filtration through a 0.2 µM filter.

The product OH-AEP was purified using a gravity-flow column with 20 mL of Q-Sepharose FF resin (GE Healthcare). The pH of the filtered solution was adjusted to 8.5 with concentrated ammonium hydroxide and then loaded onto the Q-Sepharose column that had been equilibrated with 25 mM ammonium acetate buffer pH 8.5. OH-AEP was eluted from the column by 3 CV of

25 mM ammonium acetate buffer pH 8.5. The L-ascorbate and succinate from the reaction mixture remain bound to the column under these conditions and elute at ammonium acetate concentrations of > 200 mM. The eluted fractions were analyzed by mass spectrometry (ZQ 2000 mass spectrometer, Waters) and ^{31}P-NMR spectroscopy, and fractions containing OH-AEP (the flow-through and the three 25 mM ammonium acetate elutions) were pooled and evaporated to dryness on a rotary evaporator. The solid was dissolved in a minimal volume of H_2O, and the concentration of OH-AEP was determined by ^{31}P-NMR spectroscopy using 2-AEP as an internal standard. The OH-AEP solution was aliquoted and dried using a speedvac concentrator (Savant SPD131DDA, Thermo Scientific).

The specific optical rotation of the purified OH-AEP dissolved in H_2O was determined to be $[\alpha]_D^{20}$ = –40.2 in good agreement with the previously determined literature value for *(R)*-OH-AEP (–31.4) (4).

Activity assays for PhnZ

For activity assays, the Fe^{II}/Fe^{III} state of the protein was generated by reduction of the purified protein with L-ascorbate; the fully oxidized Fe^{III}/Fe^{III} state was prepared by treatment of the protein with potassium ferricyanide ($K_3[Fe(CN)_6]$). 200 µM PhnZ was incubated in the absence of O_2 with 5 equiv. L-ascorbate (relative to the diiron cofactor), 0.2 equiv. ferricyanide, or 0.2 equiv. ferricyanide followed by 5.2 equiv. L-ascorbate in 50 mM MOPS pH 7.5, 10% (v/v) glycerol for a several minutes. EPR samples were taken to determine the yield of the mixed-valent Fe^{II}/Fe^{III} cofactor in these preparations. For the reaction in the absence of O_2, PhnZ was diluted with deoxygenated MOPS buffer to a final concentration of 10 µM, and OH-AEP substrate was added to 2 mM. The solution was incubated anaerobically under gentle stirring at room temperature. For reactions with O_2, the protein was taken out of the anoxic chamber and diluted to a final concentration of 10 µM with air-saturated MOPS buffer, OH-AEP substrate was added to 2 mM, and the reactions were continuously flushed with hydrated air under gentle stirring at room temperature.

At various time points, 480 µL aliquots were taken and quenched by addition of 4% (v/v) concentrated acetic acid. Conversion of OH-AEP to phosphate was detected by ^{31}P-NMR, as described in the ^{31}P-NMR spectroscopy section below.

PhnZ activity assays for testing O_2 incorporation into the product

Reactions contained 10 µM PhnZ enriched in the Fe^{II}/Fe^{III} state, 1 mM OH-AEP and were initiated by the addition of $^{18}O_2$- or $^{16}O_2$-saturated H_2O (~1.8 mM O_2), resulting in a final O_2

concentration of ~1.6 mM. After 1 h the reactions were stopped by addition of 0.5% (v/v) concentrated acetic acid. Precipitation was removed by centrifugation. Incorporation of oxygen from O_2 into the product glycine was detected by LC-MS, as described in the LC-MS section below.

High performance liquid chromatography – mass spectrometry (LC-MS)

LC-MS experiments were carried out on an Agilent 1200 series LC system coupled to a triple quadrupole mass spectrometer (Agilent 6410 QQQ LC/MS; Agilent Technologies). 60% (v/v) acetonitrile was added to the samples and they were filtered (0.2 µm filter) before injection on a ZIC-HILIC (Merck) column that had been equilibrated with 5% solvent A (95% H_2O, 5% acetonitrile, 0.1% formic acid) and 95% solvent B (5% H_2O, 95% acetonitrile, 0.1% formic acid). The reaction mixture was separated at 0.3 mL/min by applying a linear gradient of 5-20% A over 15 min, isocratic at 20% A for 5 min, a linear gradient of 20-70% A over 15 min, then returning to 5% A over 15 min and re-equilibrating at 5% A for 5 min. Detection of the glycine products was performed using electrospray ionization in the positive mode (ESI+) with single ion monitoring at *m/z* of 76.1 for detection of ^{16}O-glycine ($H_3N\text{-}CH_2\text{-}C^{16}O^{16}OH)^{1+}$ and *m/z* of 78.1 for detection of ^{18}O-glycine ($H_3N\text{-}CH_2\text{-}C^{16}O^{18}OH)^{1+}$. Relative quantities of ^{16}O-glycine and ^{18}O-glycine were determined by integrating the corresponding peak using the MassHunter QualitativeAnalysis Software (Agilent Technologies).

Rapid freeze-quench EPR sample preparation

An anaerobic solution of PhnZ containing 0.18 mM Fe^{II}/Fe^{III} cofactor and 3 mM (*R*)-OH-AEP was prepared and transferred to a gas-tight freeze-quench (FQ) syringe. A second syringe was filled with O_2-saturated buffer (~1.8 mM O_2, 50 mM MOPS pH 7.5, 10% (v/v) glycerol). The solution of the substrate-bound complex (PhnZ-Fe^{II}/Fe^{III}•(*R*)-OH-AEP) was mixed at 5 °C with 0.5 equivalent volumes of the O_2-saturated buffer in the FQ set-up that has previously been described (5), affording final concentrations of 0.121 mM PhnZ-Fe^{II}/Fe^{III}, 2 mM (*R*)-OH-AEP and 0.6 mM O_2. The reaction solution was aged for the desired time and then ejected into the isopentane cryo-solvent (~ -150° C) to terminate the reaction.

^{31}P-NMR spectroscopy

For ^{31}P-NMR measurements, sodium dithionite, EDTA and D_2O were added to the samples to final concentrations of 0.2 mM, 0.2 mM, and 20% (v/v), respectively. Solution ^{31}P-NMR spectra of the various phosphorous containing compounds were recorded at room temperature

in an AVX-360 Bruker spectrometer. The spectra were recorded using a 1D sequence with power-gated ^{1}H decoupling. Chemical shifts are quoted with respect to an 85% phosphoric acid solution at 0 ppm. The 85% phosphoric acid solution was transferred into a 2 mm OD quartz tube, which was then inserted into the 5 mm OD quartz NMR tube containing the solutions under investigation. NMR spectra were further processed with the freely available Spinworks (version 1.3.8.1) software (Dr. Kirk Marat, University of Manitoba, Canada).

Mössbauer spectroscopy

Mössbauer spectra were recorded on spectrometers from WEB Research (Edina, MN). The spectrometer used to acquire the weak-field spectra is equipped with a Janis SVT-400 variable-temperature cryostat. The spectrometer used to acquire the strong-field spectra is equipped with a Janis 8TMOSS-OM-12SVT variable-temperature cryostat. The external magnetic field was applied parallel to the γ-beam. All isomer shifts quoted are relative to the centroid of the spectrum of α-iron metal at room temperature. Simulation of the Mössbauer spectra was carried out by using the WMOSS spectral analysis software (www.wmoss.org, WEB Research, Edina, MN). The high-field simulations were carried out using the spin-Hamiltonian (6), in which all symbols have their usual meaning.

$$H = \mu_B \mathbf{S}\cdot\mathbf{g}\cdot\mathbf{B} + D\left(\mathbf{S_z^2} - \frac{S(S+1)}{3}\right) + E\left(\mathbf{S_x^2} - \mathbf{S_y^2}\right) + \sum_{i=1}^{2}\frac{eQV_{zz,i}}{4}\left[\mathbf{I_{z,i}^2} - \frac{I_i(I_i+1)}{3} + \frac{\eta}{3}\left(\mathbf{I_{x,i}^2} - \mathbf{I_{y,i}^2}\right)\right] + \sum_{i=1}^{2}\mathbf{S}\cdot\mathbf{A_i}\cdot\mathbf{I_i} - \sum_{i=1}^{2} g_n\mu_n\mathbf{B}\cdot\mathbf{I_i}$$

The first term corresponds to the electronic Zeeman interaction, the second and third correspond to the axial and rhombic zero field splitting, the fourth term describes the interaction between the electric field gradient and the nuclear quadrupole moment, the fifth term corresponds to the hyperfine interactions between the electronic spin and the ^{57}Fe nucleus, and the sixth term represents the nuclear Zeeman interaction. The simulations were carried out with respect to the total spin of the cluster.

EPR spectroscopy

EPR spectra were acquired on a Bruker ESP300 CW X-Band spectrometer (operating at approx. 9.48 GHz) equipped with a rectangular cavity (TE_{102}) and a continuous-flow cryostat (Oxford 910) with a temperature controller (Oxford ITC 503).

General crystallographic methods

Preliminary screening of protein crystals was performed at the X-ray crystallography facility in the Huck Institutes for the Life Sciences. Diffraction datasets for structure solution were collected at the Life Sciences Collaborative Access Team (LS-CAT) beamlines at the Advanced Photon Source. All datasets were indexed, integrated, and scaled using the HKL 2000 software package (7). Model building was accomplished in Coot (8), and refinement was carried out in PHENIX (9). All data collection and refinement statistics are reported in Table S1. Structure validation was performed with Molprobity. Figures were generated with the PyMOL Molecular Graphics System (Schrödinger, LLC), and electron density maps were calculated with PHENIX (9).

Determination of the structure of citrate-bound PhnZ

N-terminally His_6-tagged PhnZ overexpressed from pRSET_*phnZ* was prepared for crystallographic analysis as described in the protein production and purification section. An additional size-exclusion chromatography step (Sephacryl-200 gel filtration column, GE Healthcare) was included using 50 mM MOPS pH 7.5, 10% (v/v) glycerol as running buffer. Hexagonal prism-shaped crystals of PhnZ (12 mg/mL) appeared after one week of incubation at room temperature using the sitting drop vapor diffusion method with 0.1 M HEPES pH 7.5, 1.4 M trisodium citrate as the precipitant. Crystals were mounted on rayon loops for data collection and flash-frozen by direct plunge into liquid nitrogen with no further cryoprotection. The structure was solved by single-wavelength anomalous diffraction (SAD) phasing using a dataset collected at the Fe X-ray absorption peak. The phases were determined with autoSHARP (10) using the two active site Fe ions (Table S1). From the resulting electron density maps, an initial model was generated with Buccaneer (11). An additional high-resolution native dataset was used to generate and refine the final model. The final model consists of PhnZ residues 1-66, residues 72-187, two Fe ions, one citrate anion, one bridging hydroxo group and 153 water molecules. No electron density is observed for the N-terminal affinity tag and for a surface loop (residues 66-72) near the active site. The occupancies of two metal ions were refined with PHENIX and both sites are modeled at nearly full (92%) occupancy. Ramachandran plots show that 100% of the residues are in allowed and additionally allowed regions.

Determination of the structure of OH-AEP-bound PhnZ

The *phnZ* gene was PCR amplified from the pRSET_*phnZ* plasmid and subcloned into a pET26b vector using *NdeI* and *XhoI* restriction sites resulting in the plasmid pET26b_*phnZ*

encoding the *phnZ* gene with a C-terminal His_6-tag. This protein was overexpressed in *E. coli* BL21 cells that had been transformed with pET26b_*phnZ*. Cultures were grown at 30 °C in enriched LB medium supplemented with kanamycin (0.05 mg/mL) to an OD_{600} of 0.7, followed by IPTG induction (0.1 mM) for 16 hours at 30 °C. The protein was purified and prepared for crystallization trials as described for the N-terminally tagged protein overexpressed from pRSET_*phnZ.*

Crystals of C-terminally His_6-tagged PhnZ with bound (*R*)-OH-AEP were prepared from a solution containing both the enzyme (14 mg/mL) and the substrate (8 molar equiv.) that was preincubated for 20 minutes on ice prior to setup of the crystallization trials. Plate-like crystals grew overnight in sitting drop vapor diffusion trays with 0.1 M sodium acetate pH 4.6, 0.2 M ammonium sulfate, and 25% (w/v) PEG 4000 as the precipitant. Crystals were mounted on rayon loops for data collection and incrementally transferred (5% increase in glycerol) into a final cryoprotection solution of 0.1 M sodium acetate pH 4.6, 0.2 M ammonium sulfate, 25% (w/v) PEG 4000 and 25% (v/v) glycerol.

The structure was solved by molecular replacement using PHASER (12) with the citrate-bound PhnZ structure as the search model. Four substrate-bound PhnZ molecules are present in the asymmetric unit. The coordinates for (*R*)-OH-AEP were generated using the PRODRG server (13). The final model consists of residues 4-65 and residues 70-187 in chains A, B, and E; residues 4-64 and residues 70-187 in chain D; eight Fe ions; and four (*R*)-OH-AEP molecules. No electron density was observed in any of the four PhnZ molecules for residues 1-3, residues 66-69, or the C-terminal His_6 tag. The occupancies of the substrate atoms and metal ions were refined in PHENIX and are modeled at 100% occupancy in the final model. Ramachandran plots show that 99.8% of the residues are in allowed and additionally regions.

Phylogenetic analysis

The Basic Local Alignment Search Tool (BLAST) was used to perform similarity searches through the NCBI BLAST webpage interface (http://www.ncbi.nlm.nih.gov/BLAST/) (14). The retrieved sequences were initially grouped on the basis of similarity relationships and the genomic contexts of their encoding genes. The sequences were further culled by requiring that each contain at least the six conserved residues necessary for coordinating a dinuclear cluster (i.e. four histidines and two glutamates). Each selected sequence was examined for completeness and length. Approximately 8 sequences from each group were chosen, so as to have equal representations from each group within the phylogenetic tree and avoid bias. The amino acid sequences of each group were aligned using the MAFFT (version is 7.03,

http://mafft.cbrc.jp/alignment/software/) online webserver (15) and the ClustalW algorithm as implemented in the MEGA 5.2 software (16, 17). For the construction of the tree, all sequences were further re-aligned together. Neighbor joining (NJ) (18), minimum evolution and maximum likelihood (19) trees were constructed using the respective algorithms in the MEGA software package and the MAFFT online server as well as the older software ClustalX2 (20). Similar trees were obtained with the different methods. The robustness of the trees was further confirmed by using the bootstrap method with 1000 replications.

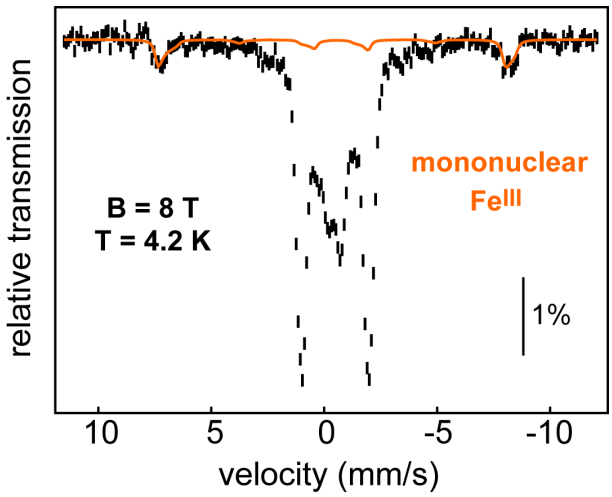

Figure S1. 4.2-K Mössbauer spectrum of the aerobically isolated PhnZ recorded in a wide range (~ ±12 mm/s) of Doppler velocities. An external magnetic field of 8 T applied parallel to the γ-beam. The orange solid line represents a simulation of the mononuclear high-spin Fe^{III} contaminant(s). Its integrated intensity corresponds to 7% of the total Fe species in the sample. The simulation was carried out using the spin-Hamiltonian formalism with the following parameters: S = 5/2, D = -1.0 cm^{-1}, E/D = 0.33, g = 2.0, δ = 0.55 mm/s, ΔE_Q = -1 mm/s, η = -2.5, $A_{iso}/(g_N \beta_N)$ = -22.2 T.

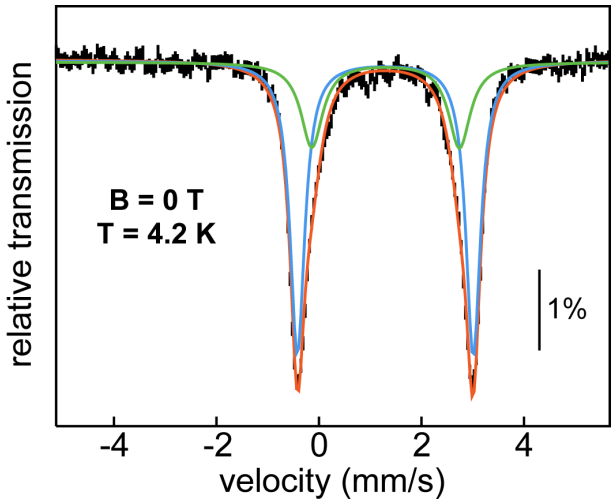

Figure S2. 4.2-K/0-T Mössbauer spectrum of the dithionite-reduced form of PhnZ. The experimental spectrum (black vertical bars) is fit by two sets of quadrupole doublets with parameters δ_1 = 1.30 mm/s, ΔE_{Q1} = 3.43 mm/s (blue solid line), δ_2 = 1.3 mm/s and ΔE_{Q2} = 2.83 mm/s (green solid line) and a Lorentzian line shape. The overall fit (summation) is shown as a red solid line.

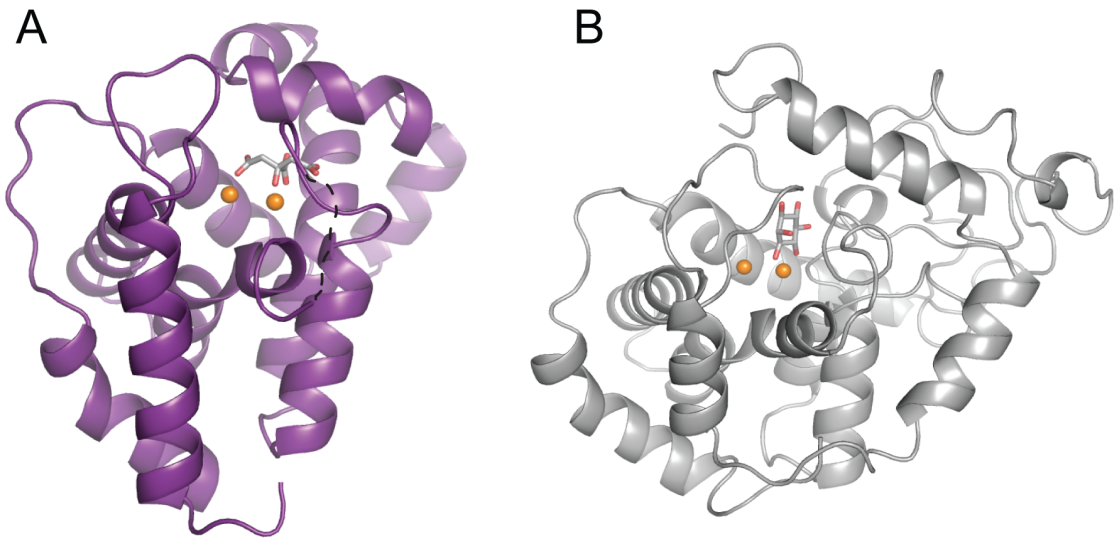

Figure S3. Comparison of the overall structures of citrate-bound PhnZ (A) and *M. musculus* MIOX (PDB accession code 2HUO) (B). A disordered region in PhnZ is represented by a black dashed line. The Fe ions in both structures are shown as orange spheres, and the substrate and citrate molecules are shown in stick format.

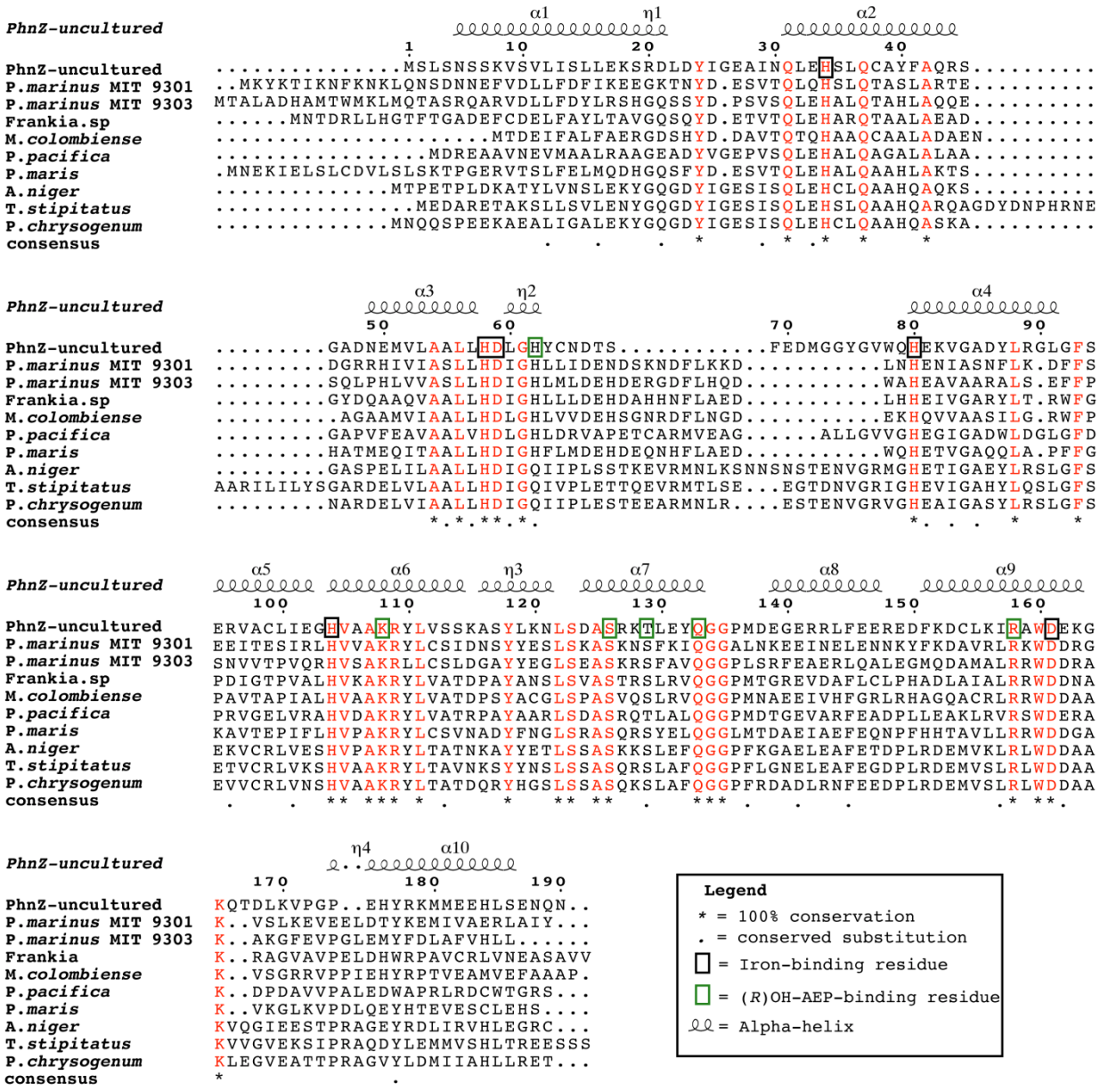

Figure S4. Multiple sequence alignment of PhnZ-like sequences.

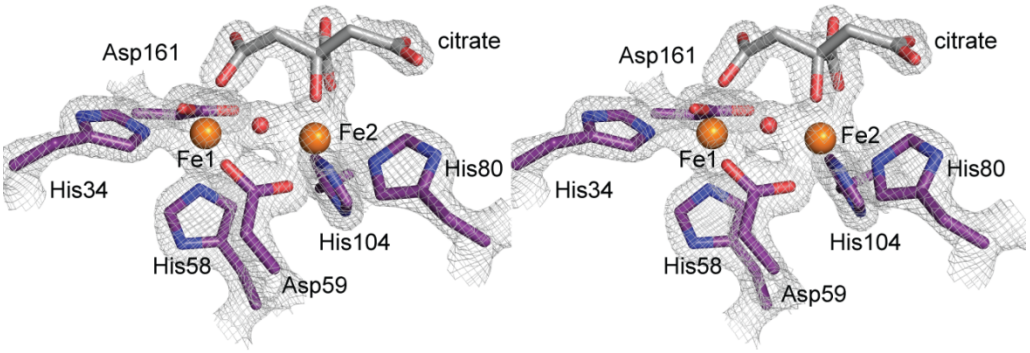

Figure S5. Stereoview of the $2F_o$-F_c electron density map (gray mesh contoured at 2.0σ) for the diiron site and bound citrate molecule in the high-resolution PhnZ X-ray structure. The Fe ions are shown as orange spheres and the bridging oxygen species is shown as a red sphere. The side chains of the coordinating residues are shown in stick format and colored by atom type.

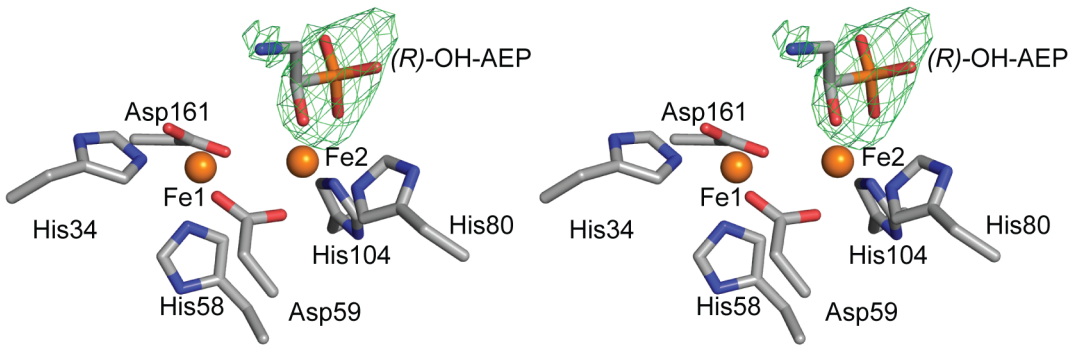

Figure S6. Stereoview of an omit map (green mesh contoured at 3.0σ) showing the electron density for the substrate molecule in chain A of the substrate-bound PhnZ structure. The Fe ions are shown as orange spheres and the side chains of the coordinating residues are shown in stick format and colored by atom type. The substrate molecule was modeled at 100% occupancy in all monomers with minor differences in the orientation of the amino group.

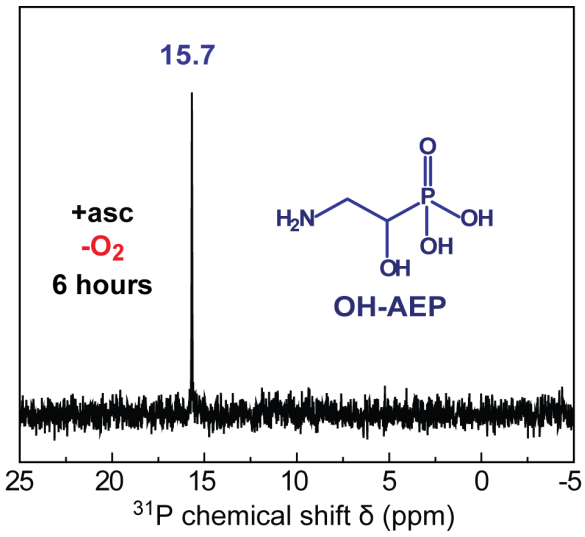

Figure S7. ^{31}P-NMR spectrum of a sample containing 10 μM PhnZ, 2 mM OH-AEP and 5 equiv. of L-ascorbate that was incubated in the anoxic chamber for 6 hours at ambient temperature. The absence of phosphate product establishes that O_2 is required for the PhnZ reaction.

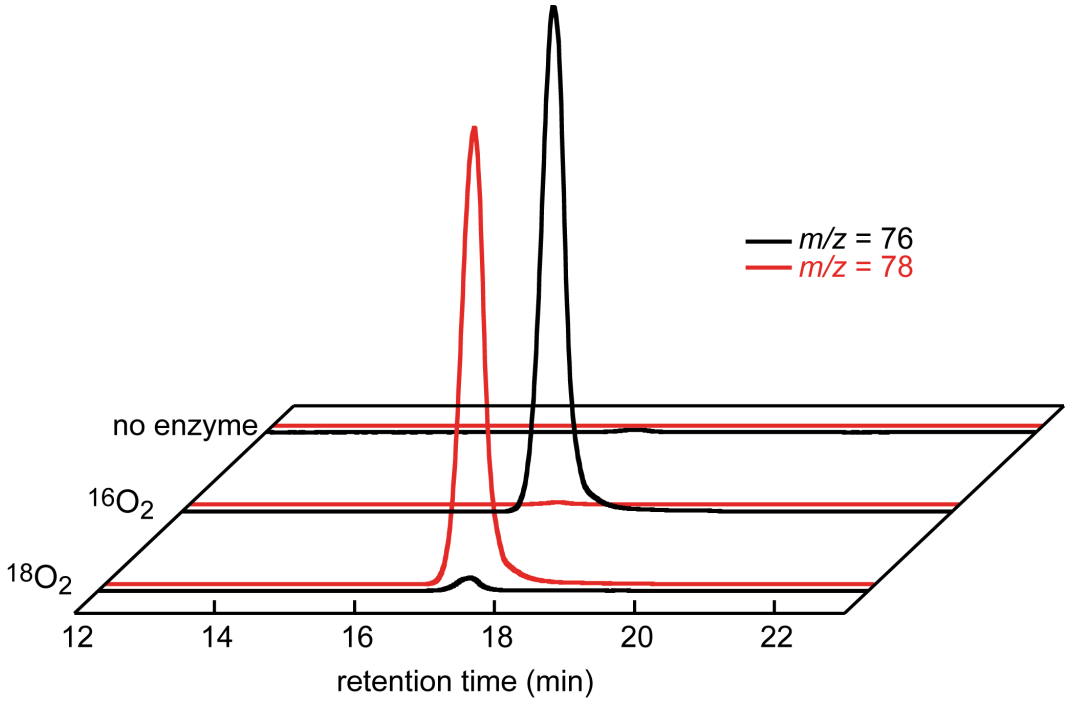

Figure S8. Incorporation of an O-atom from O_2 into glycine demonstrated by LC-MS single-ion-monitoring (SIM) chromatograms of PhnZ reactions in the presence of $^{16}O_2$ and $^{18}O_2$ and of a no enzyme control. SIM chromatograms for *m/z* = 76, corresponding to ^{16}O-glycine $(H_3N\text{-}CH_2\text{-}C^{16}O^{16}OH)^{1+}$, are shown in black, and those for *m/z* = 78, corresponding to ^{18}O-glycine $(H_3N\text{-}CH_2\text{-}C^{16}O^{18}OH)^{1+}$ are shown in red. The nearly complete (98%) incorporation of ^{18}O from $^{18}O_2$ into the glycine product establishes that PhnZ is an oxygenase.

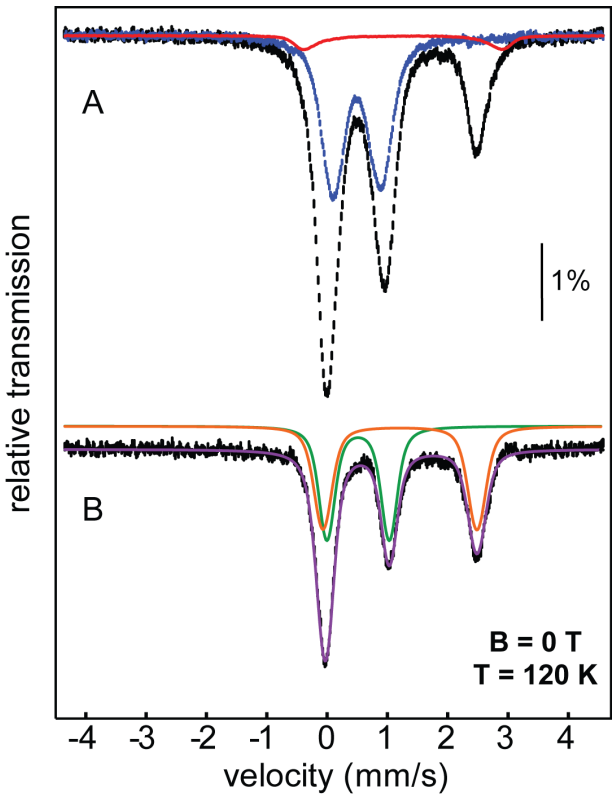

Figure S9. 120-K/0-T Mössbauer spectra of PhnZ. (A) Spectrum of the aerobically isolated PhnZ following treatment in the absence of O_2 with excess L-ascorbate, which was then removed using a PD-10 desalting column (black). The spectrum contains an upper limit of 4% of the Fe^{II}/Fe^{II} state (red) and approximately 46% of the Fe^{III}/Fe^{III} form (blue). Subtraction of these contributions yields the reference spectrum of the mixed-valent Fe^{II}/Fe^{III} form (B; black). The individual contributions of the Fe^{III} site (δ = 0.51 mm/s, ΔE_Q=1.03 mm/s) and the Fe^{II} site (δ = 1.20 mm/s, ΔE_Q = 2.55 mm/s) are shown in green and orange, respectively. The summation of these contributions is shown in purple.

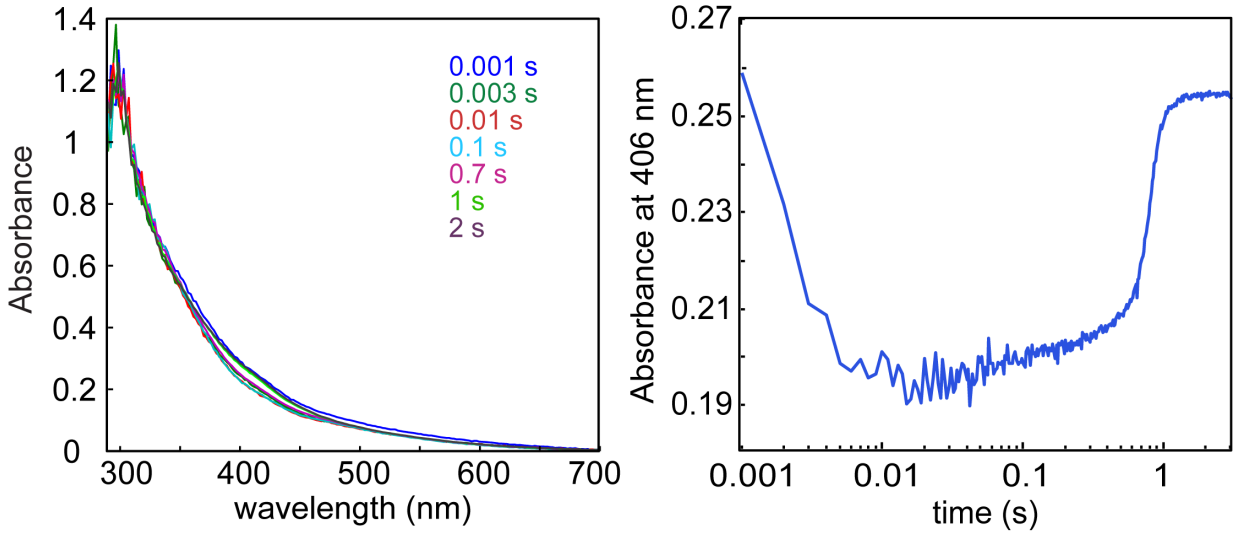

Figure S10. Reaction of PhnZ-Fe^{II}/Fe^{III}•OH-AEP with O_2 at 5 °C monitored by stopped-flow absorption spectroscopy. (Left) Absorption spectra at the reaction times shown in the figure. (Right) Kinetics of the absorbance at 406 nm. Concentrations after mixing were 0.07 mM PhnZ-Fe^{II}/Fe^{III}, 1.5 mM OH-AEP, and ~ 0.9 mM O_2 in 50 mM MOPS buffer pH 7.5.

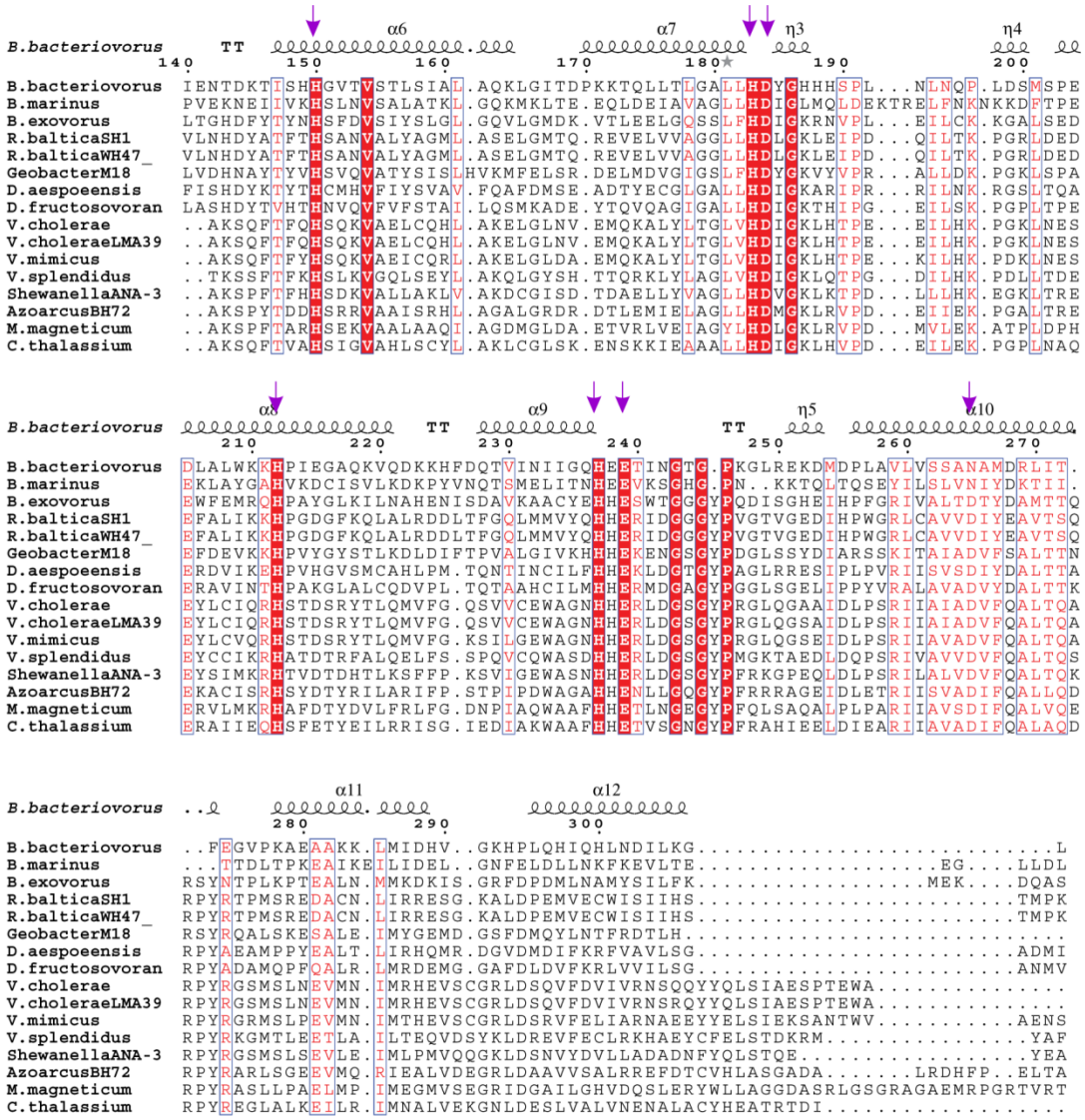

Figure S11. Multiple sequence alignment of the proteins in the HD-GYP and HD-[HD-GYP] clades starting from residue 140. Residues that coordinate the metal ions are indicated with purple arrows.

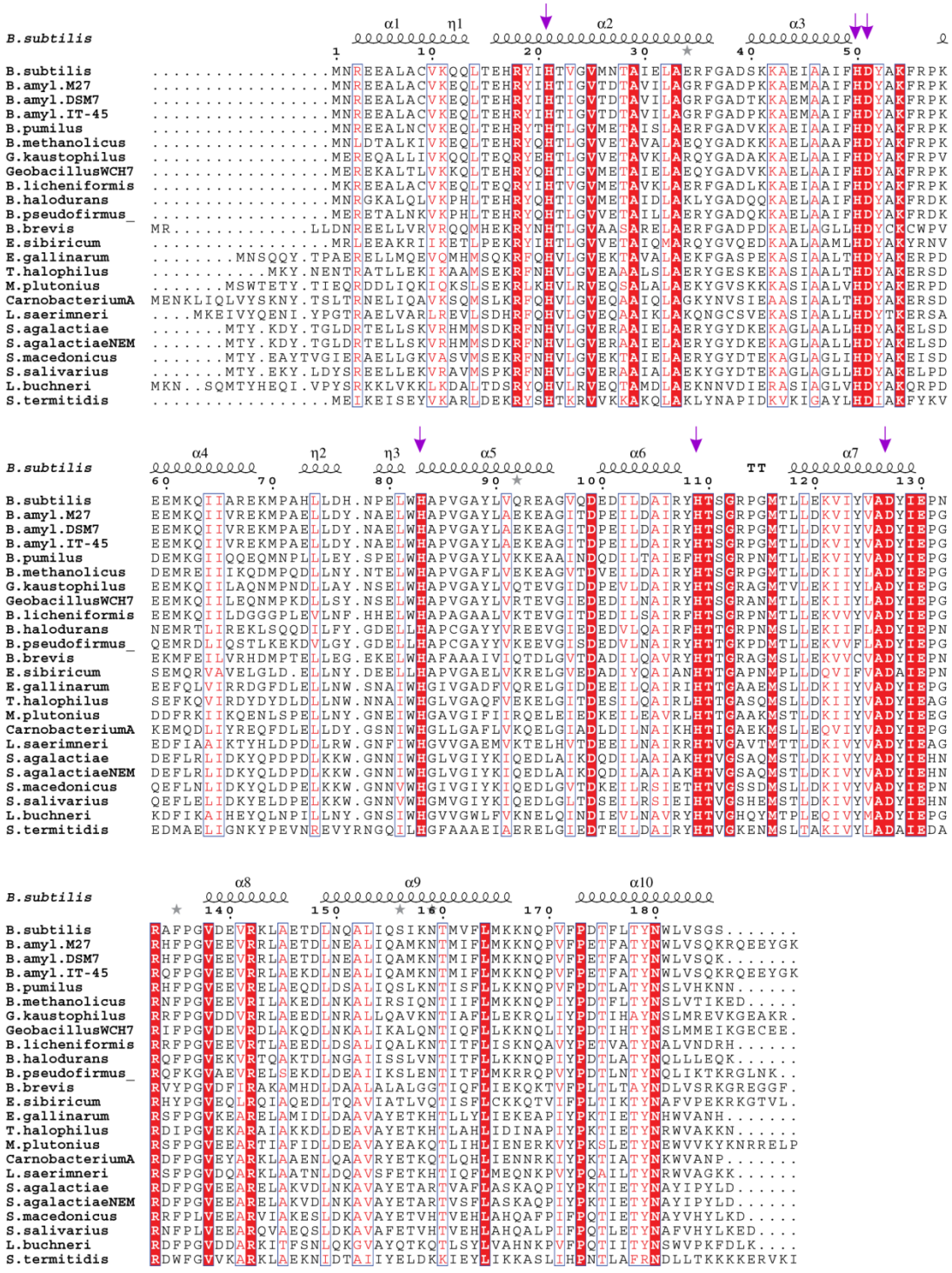

Figure S12. Multiple sequence alignment of the proteins in the YqeK clade. Residues that coordinate the metal ions are indicated with purple arrows.

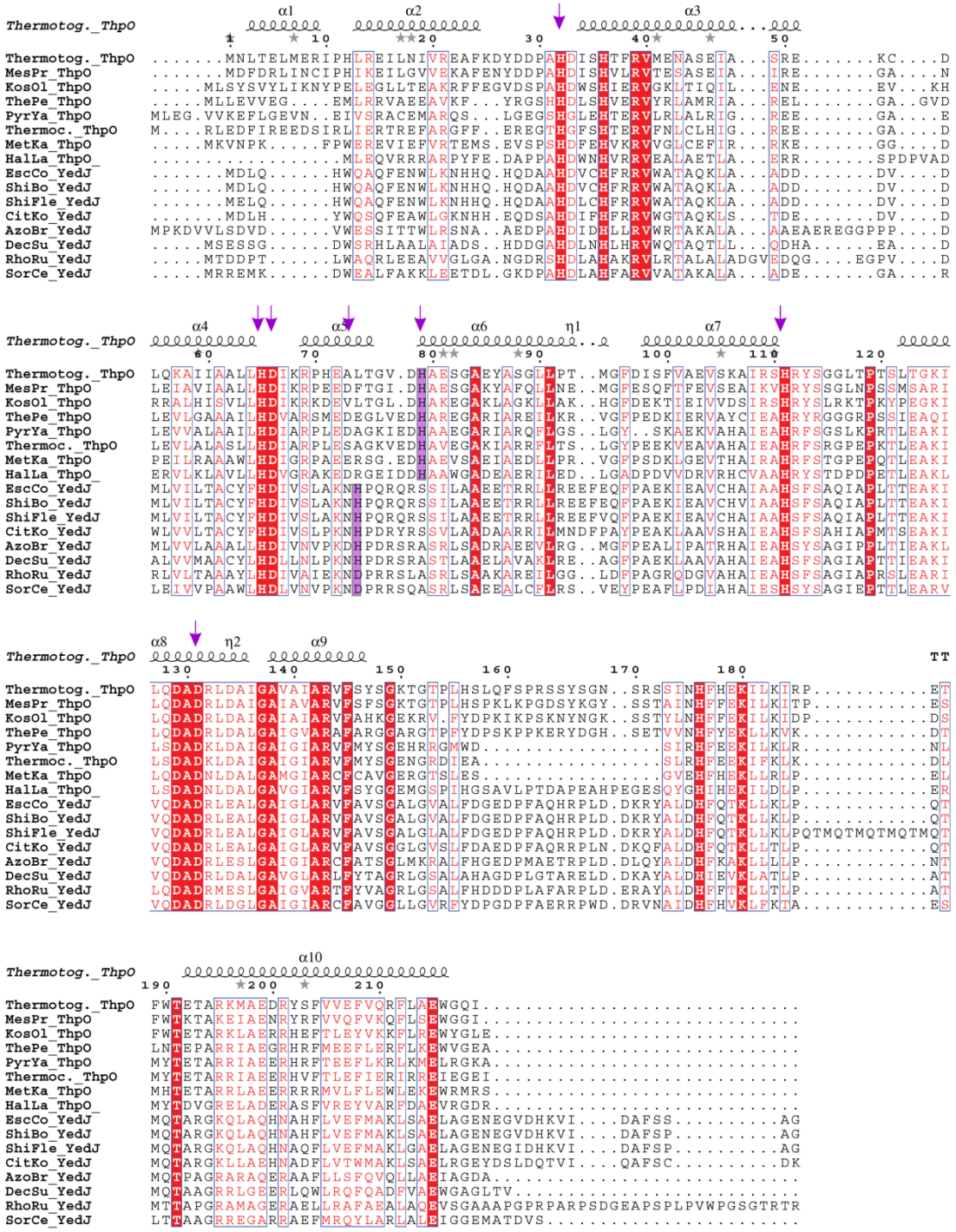

Figure S13. Multiple sequence alignment of the proteins in the ThpO and YedJ clades. Residues that coordinate the metal ions are indicated with purple arrows. Purple shaded boxes indicate the 5th His ligands in ThpO and YedJ respectively.

Table S1. Data collection and refinement statistics for the citrate-bound and substrate-bound (OH-AEP) PhnZ X-ray crystal structures.

	PhnZ-citrate	PhnZ-citrate (ano)	PhnZ-substrate
Data collection			
Wavelength (Å)	0.98	1.72	0.98
Space group	$P3_121$	$P3_121$	$C2$
Unit cell dimensions			
a, b, c (Å)	68.18, 68.18, 98.09	67.97, 67.97, 98.30	148.75, 165.42, 109.35
Resolution (Å)	50.00-1.85 (1.88-1.85)*	50.00-2.92 (2.97-2.92)*	30.00-2.98 (3.05-2.98)*
R_{sym} or R_{merge}	0.063 (0.817)	0.343 (0.163)	0.126 (0.372)
I / σ(I)	49.6 (3.1)	16.4 (36.2)	13.06 (4.16)
Completeness (%)	99.94 (99.40)	100 (100)	93.5 (96.9)
Redundancy	10.8 (9.8)	20.7 (20.1)	5.9 (5.6)
Refinement			
Resolution range (Å)	50.00-1.85		30.00-2.98
No. unique reflections	23752		16580
R_{work} / R_{free}	0.1875/0.2118		0.278/0.333
No. atoms	1593		5767
Protein	1434		5727
Ligand/ions	14		40
Water	154		N/A
Avg. *B*-factor			
Protein	34.20		67.40
Ligand/ions	26.70		52.80
Water	43.20		N/A
r.m.s deviations			
Bond lengths (Å)	0.006		0.008
Bond angles (°)	0.94		0.452

*Values in parentheses report statistics for the highest-resolution shell

Table S2. Proteins used for the phylogenetic analysis.

Accession code	NCBI Annotation	Organism
ACU83550.1	predicted HD phosphohydrolase PhnZ	uncultured bacterium HF130_AEPn_1
YP_001091480.1	hypothetical protein P9301_12561	*Prochlorococcus marinus* str. MIT 9301
YP_001017139.1	hypothetical protein P9303_11251	*Prochlorococcus marinus* str. MIT 9303
YP_481098.1	hypothetical protein Francci3_1995	*Frankia* sp. CcI3
ZP_08717929.1	hypothetical protein MCOL_20456	*Mycobacterium colombiense* CECT 3035
ZP_01905457.1	HDIG domain protein	*Plesiocystis pacifica* SIR-1
ZP_01854986.1	hypothetical protein PM8797T_07614	*Planctomyces maris* DSM 8797
XP_001399948.1	hypothetical protein ANI_1_2760024	*Aspergillus niger* CBS 513.88
XP_002479453.1	conserved hypothetical protein	*Talaromyces stipitatus* ATCC 10500
XP_002565218.1	hypothetical protein Pc22g12750	*Penicillium chrysogenum* Wisconsin 54-1255
YP_006563750.1	metal-dependent phosphohydrolases-like protein	*Phaeobacter gallaeciensis* 2.10
ZP_05080776.1	conserved hypothetical protein	*Rhodobacterales bacterium* Y4I
ZP_05786163.1	conserved hypothetical protein	*Silicibacter lacuscaerulensis* ITI-1157
ZP_05087911.1	conserved hypothetical protein	*Ruegeria* sp. R11
YP_004014535.1	phosphonate degradation operons associated HDIG domain-containing protein	*Frankia* sp. EuI1c
YP_004142411.1	hypothetical protein	*Mesorhizobium ciceri biovar biserrulae* WSM1271
ZP_01074753.1	hypothetical protein MED121_17544	*Marinomonas* sp. MED121
ZP_01754854.1	hypothetical protein RSK20926_22209	*Roseobacter* sp. SK209-2-6
ZP_10649542.1	phosphonate degradation operons associated HDIG domain protein	*Pseudomonas* sp. GM50
ZP_11114572.1	phosphonate degradation operons associated HDIG domain protein	*Pseudomonas mandelii* JR-1
YP_007032156.1	metal-dependent phosphohydrolase	*Pseudomonas* sp. UW4
ZP_18348829.1	phosphonate degradation operons associated HDIG domain protein	*Pseudomonas fluorescens* R124
YP_262944.1	phosphonate degradation operons associated HDIG domain protein	*Pseudomonas protegens* Pf-5
ZP_10174257.1	phosphonate degradation operons associated HDIG domain protein	*Pseudomonas chlororaphis* O6
ZP_10142158.1	phosphonate degradation operons associated HDIG domain protein	*Pseudomonas synxantha* BG33R
AAV65817.1	*myo*-inositol oxygenase	*Rattus norvegicus*
XP_003509608.1	PREDICTED: inositol oxygenase-like	*Cricetulus griseus*
AAF25204.1	*myo*-inositol oxygenase	*Homo sapiens*
NP_001124754.1	inositol oxygenase	*Pongo abelii*
XP_003281515.1	PREDICTED: inositol oxygenase-like	Nomascus leucogenys
XP_003461613.1	PREDICTED: inositol oxygenase-like	*Cavia porcellus*
XP_001490312.3	PREDICTED: inositol oxygenase-like	*Equus caballus*(horse)
AAK00766.1	kidney-specific protein 32	*Homo sapiens*
CAJ75704.1	predicted HD superfamily hydrolase	uncultured *Thermotogales* bacterium
AFK07215.1	putative domain HDIG-containing protein	*Mesotoga prima* MesG1.Ag.4.2
YP_002940461.1	metal-dependent phosphohydrolase	*Kosmotoga olearia* TBF 19.5.1
YP_920563.1	metal-dependent phosphohydrolase	*Thermofilum pendens* Hrk 5
NP_614753.1	HD superfamily hydrolase	*Methanopyrus kandleri* AV19
YP_004624251.1	metal-dependent phosphohydrolase, HD superfamily	*Pyrococcus yayanosii* CH1
YP_006424365.1	hypothetical protein containing HD domain 1	*Thermococcus* sp. CL1
ZP_09946302.1	metal-dependent phosphohydrolase	*Halobiforma lacisalsi* AJ5
NP_416471.1	predicted hydrolase, HD superfamily	*Escherichia coli* str. K-12 substr. MG1655
YP_407527.1	hypothetical protein SBO_1046	*Shigella boydii* Sb227
EGM61578.1	HD domain protein	*Shigella flexneri* J1713
YP_001452563.1	hypothetical protein CKO_00980	*Citrobacter koseri* ATCC BAA-895
CCD01718.1	putative metal-dependent phosphohydrolase	*Azospirillum brasilense* Sp245
YP_005029269.1	unnamed protein product	*Dechlorosoma suillum* PS

YP_001615272.1	unnamed protein product	*Sorangium cellulosum* 'So ce 56'
YP_427146.1	metal-dependent phosphohydrolase, HD region	*Rhodospirillum rubrum* ATCC 11170
P54456.1	Uncharacterized protein yqeK	*Bacillus subtilis* subsp. *subtilis* str. 168
YP_148374.1	hypothetical protein GK2521	*Geobacillus kaustophilu*s HTA426
YP_079904.1	hypothetical protein BL02082	*Bacillus licheniformis* ATCC 14580
YP_001487526.1	*yqeK* gene product	*Bacillus pumilus* SAFR-032
YP_002771473.1	hypothetical protein BBR47_19920	*Brevibacillus brevis* NBRC 100599
YP_001813266.1	metal-dependent phosphohydrolase	*Exiguobacterium sibiricum* 255-15
ZP_05648832.1	HD domain-containing protein	*Enterococcus gallinarum* EG2
ZP_03943580.1	HD superfamily hydrolase	*Lactobacillus buchneri* ATCC 11577
NP_242193.1	hypothetical protein BH1327	*Bacillus halodurans* C-125
YP_003427593.1	hypothetical protein BpOF4_13250	*Bacillus pseudofirmus* OF4
YP_002950417.1	metal-dependent phosphohydrolase	*Geobacillus* sp. WCH70
ZP_11547518.1	YqeK	*Bacillus methanolicus* MGA3
ZP_16170044.1	2',3'-cyclic-nucleotide 2'-phosphodiesterase	*Bacillus amyloliquefaciens* subsp. *plantarum* M27
ZP_17179708.1	YqeK	*Bacillus amyloliquefaciens* IT-45
YP_003921057.1	hydrolase	Bacillus amyloliquefaciens DSM 7
YP_003307575.1	kidney-specific protein 32	*Sebaldella termitidis* ATCC 33386
NP_688652.1	hypothetical protein SAG1661	*Streptococcus agalactiae* 2603V/R
NP_736140.1	hypothetical protein gbs1705	*Streptococcus agalactiae* NEM316
YP_005095370.1	hydrolase	*Streptococcus macedonicus* ACA-DC 198
ZP_12658042.1	putative HD superfamily hydrolase	*Streptococcus salivarius* M18
YP_004886756.1	hypothetical protein TEH_12650	*Tetragenococcus halophilus* NBRC 12172
ZP_19196683.1	hypothetical protein D271_06905	*Lactobacillus saerimneri* 30a
YP_004455861.1	HAD superfamily hydrolase	*Melissococcus plutonius* ATCC 35311
ZP_02184981.1	HD domain protein	*Carnobacterium* sp. AT7
NP_968683.1	hypothetical protein Bd1817	*Bdellovibrio bacteriovorus* HD100
YP_005036194.1	unnamed protein product	*Bacteriovorax marinus* SJ
YP_007644848.1	HD-GYP hydrolase domain-containing protein	*Bdellovibrio exovorus* JSS
YP_004196908.1	metal-dependent phosphohydrolase	*Geobacter* sp. M18
YP_004119802.1	metal-dependent phosphohydrolase	*Desulfovibrio aespoeensis* Aspo-2
ZP_07334137.1	metal-dependent phosphohydrolase	*Desulfovibrio fructosovorans* JJ
NP_864187.1	response regulator	*Rhodopirellula baltica* SH 1
EGF24277.1	HD-GYP domain-containing protein	*Rhodopirellula baltica* WH47
NP_233069.1	hypothetical protein VCA0681	*Vibrio cholerae* O1 biovar El Tor str. N16961
YP_005632344.1	HDIG domain-containing protein	*Vibrio cholerae* LMA3984-4
YP_002395757.1	hypothetical protein VS_II1179	*Vibrio splendidus* LGP32
WP_005508357.1	hypothetical protein	*Vibrio mimicus*
YP_868720.1	metal-dependent phosphohydrolase	*Shewanella* sp. ANA-3
YP_933792.1	HD-domain-containing protein	*Azoarcus* sp. BH72
YP_423590.1	HD-GYP domain-containing protein	*Magnetospirillum magneticum* AMB-1
YP_001996362.1	metal dependent phosphohydrolase	*Chloroherpeton thalassium* ATCC 35110
NP_416794.1	5'-nucleotidase YfbR	*Escherichia coli* str. K-12 substr. MG1655
EIE57001.1	5'-nucleotidase YfbR	*Escherichia coli* AI27
EHS94221.1	UPF0207 protein YfbR	*Klebsiella oxytoca* 10-5245
YP_003742460.1	unnamed protein product	*Erwinia billingiae* Eb661
YP_005401021.1	unnamed protein product	*Rahnella aquatilis* HX2
AFH92378.1	5'-nucleotidase	*Providencia stuartii* MRSN 2154
YP_005634320.1	unnamed protein product	*Vibrio cholerae* LMA3984-4
YP_002506133.1	unnamed protein product	*Clostridium cellulolyticum* H10

REFERENCES

1. Gasteiger E. HC, Gattiker A., Duvaud S., Wilkins M.R., Appel R.D., Bairoch A. (2005) Protein Identification and Analysis Tools on the ExPASy Server. *The Proteomics Protocols Handbook*, ed Walker JM (Humana Press), pp 571-607.
2. Bollinger JM, Jr. (1993) On the chemical mechanism of assembly of the tyrosyl radical-dinuclear iron cluster cofactor of *E.coli* ribonucleotide reductase. Ph. D. (Massachusetts Institute of Technology).
3. Dassama LMK, Boal AK, Krebs C, Rosenzweig AC, & Bollinger JM, Jr. (2012) Evidence that the β subunit of *Chlamydia trachomatis* ribonucleotide reductase is active with the manganese ion of its manganese(IV)/iron(III) cofactor in site 1. *J. Am. Chem. Soc.* 134(5):2520-2523.
4. Hammerschmidt F & Völlenkle H (1989) Absolute Konfiguration der (2-Amino-1-hydroxyethyl)phosphonsäure aus *Acanthamoeba castellanii* (Neff) - Darstellung der Phosphonsäure-Analoga von (+)- und (-)-Serin. *Liebigs Ann. Chem.* 1989(6):577-583.
5. Bollinger JM, Jr.*, et al.* (1995) Use of rapid kinetics methods to study the assembly of the diferric-tyrosyl radical cofactor of *E. coli* ribonucleotide reductase. *Methods Enzymol.* 258:278-303.
6. Münck E (2000) Aspects of ^{57}Fe Mössbauer spectroscopy. *Physical Methods in Bioinorganic Chemistry*, ed Que L, Jr. (University Science Books, Sausalito, CA), pp 287-319.
7. Otwinowski Z & Minor W (1997) Processing of X-ray diffraction data collected in oscillation mode. 276:307-326.
8. Emsley P, Lohkamp B, Scott WG, & Cowtan K (2010) Features and development of Coot. *Acta Crystallogr. D Biol. Crystallogr.* 66(Pt 4):486-501.
9. Adams PD*, et al.* (2010) PHENIX: a comprehensive Python-based system for macromolecular structure solution. *Acta Crystallogr. D Biol. Crystallogr.* 66(Pt 2):213-221.
10. Vonrhein C, Blanc E, Roversi P, & Bricogne G (2007) Automated structure solution with autoSHARP. *Methods Mol. Biol.* 364:215-230.
11. Cowtan K (2006) The Buccaneer software for automated model building. 1. Tracing protein chains. *Acta Crystallogr. D Biol. Crystallogr.* 62(Pt 9):1002-1011.
12. McCoy AJ, Grosse-Kunstleve RW, Storoni LC, & Read RJ (2005) Likelihood-enhanced fast translation functions. *Acta Crystallogr.* D61(4):458-464.
13. Schüttelkopf AW & van Aalten DM (2004) PRODRG: a tool for high-throughput crystallography of protein-ligand complexes. *Acta Crystallogr. D Biol. Crystallogr.* 60(Pt 8):1355-1363.
14. Altschul SF, Gish W, Miller W, Myers EW, & Lipman DJ (1990) Basic local alignment search tool. *J. Mol. Biol.* 215(3):403-410.
15. Katoh K & Standley DM (2013) MAFFT multiple sequence alignment software version 7: improvements in performance and usability. *Mol. Biol. Evol.* 30(4):772-780.
16. Thompson JD, Higgins DG, & Gibson TJ (1994) CLUSTAL W: improving the sensitivity of progressive multiple sequence alignment through sequence weighting, position-specific gap penalties and weight matrix choice. *Nucleic Acids Res.* 22(22):4673-4680.

17. Tamura K*, et al.* (2011) MEGA5: molecular evolutionary genetics analysis using maximum likelihood, evolutionary distance, and maximum parsimony methods. *Mol. Biol. Evol.* 28(10):2731-2739.
18. Saitou N & Nei M (1987) The neighbor-joining method: a new method for reconstructing phylogenetic trees. *Mol. Biol. Evol.* 4(4):406-425.
19. Takahashi K & Nei M (2000) Efficiencies of fast algorithms of phylogenetic inference under the criteria of maximum parsimony, minimum evolution, and maximum likelihood when a large number of sequences are used. *Mol. Biol. Evol.* 17(8):1251-1258.
20. Larkin MA*, et al.* (2007) Clustal W and Clustal X version 2.0. *Bioinformatics* 23(21):2947-2948.